Synthesis and evaluation of carbon-coated Fe_2O_3 loaded on graphene nanosheets as an anode material for high performance lithium ion batteries

CrossMark

Gang Wang [a], Hui Wang [b,*], Shaobo Cai [b], Jintao Bai [a], Zhaoyu Ren [a], Jinbo Bai [c]

[a] National Key Laboratory of Photoelectric Technology and Functional Materials (Culture Base), National Photoelectric Technology and Functional Materials & Application International Cooperation Base, Institute of Photonics & Photon-Technology, Northwest University, Xi'an 710069, PR China
[b] Key Laboratory of Synthetic and Natural Functional Molecule Chemistry, Ministry of Education, College of Chemistry & Materials Science, Northwest University, Xi'an 710069, PR China
[c] Lab. MSS/MAT, CNRS UMR 8579, Ecole Centrale Paris, 92295 Chatenay Malabry, France

HIGHLIGHTS

- Fe_2O_3@C/GNs hybrid material was constructed by a two step route.
- Fe_2O_3@C/GNs electrode shows superior electrochemical performance.
- The integrity of Fe_2O_3@C/GNs electrode is maintained during the continuous cycles.

ARTICLE INFO

ABSTRACT

A hybrid material of carbon-coated Fe_2O_3 submicro-particles loaded on graphene nanosheets (Fe_2O_3@C/GNs) is prepared by a two step route including a hydrothermal and a subsequent glucose impregnation-pyrolysis process. The obtained material is composed of GNs and ~ 400 nm size Fe_2O_3 particles coated by thin carbon layer with a thickness of 5 nm. As an anode material for lithium ion batteries, Fe_2O_3@C/GNs hybrid shows an improved electrochemical performance in the initial coulombic efficiency (71%), reversible capacity (900 mA h g^{-1} after 50 cycles at a current of 200 mA g^{-1}) and capacity retention rate (82% after 50 cycles). This result is much better than the synthesized bare Fe_2O_3 and Fe_2O_3/GNs electrodes. In addition to the contribution of GNs, the carbon-coated layer around Fe_2O_3 particles is believed to be a key factor to improve the electrochemical performance of Fe_2O_3.

© 2013 Elsevier B.V. All rights reserved.

1. Introduction

Lithium ion batteries (LIBs) have attracted great interest as a promising energy source and have been the most utilized batteries in the portable electronic market due to their high energy and power density [1,2]. Currently, the commercial anode material of choice is graphite, which has the advantages of long cycle life and low cost. However, its low theoretical capacity of 372 mA h g^{-1} can not satisfy future requirements of the electronic devices [3]. For the purpose of improving the electrochemical performance of LIBs, considerable efforts have been made in finding new electrode materials, which always have higher energy density compared with the existing system [4–6]. Among the available anode materials,

Fe_2O_3, as the most stable iron oxide, has attracted special attention recently mainly because of its relatively high theoretical capacity, high corrosion resistance, environmentally benign and low processing cost [7]. The electrochemical conversion mechanism of Fe_2O_3 with lithium ion can be expressed as Equation (1):

$$Fe_2O_3 + 6Li^+ + 6e^- \rightleftharpoons 2Fe + 3Li_2O \tag{1}$$
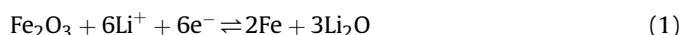
Each formula unit of Fe_2O_3 can react with six lithium ion to form a material containing Fe clusters embedded in amorphous Li_2O matrix, which reversibly converts to Fe_2O_3 on charging process [8]. On the basis of the reversible reaction (1), the theoretical lithium storage capacity of Fe_2O_3 could be approximately 1005 mA h g^{-1}, which is more than a factor of 2.5 greater than that of widely used graphite. However, widespread use of the high capacity anode material is still largely hampered. This is because most Fe_2O_3 electrodes failed to

* Corresponding author. Tel.: +86 29 8836 3115; fax: +86 29 8830 3798.
E-mail address: huiwang@nwu.edu.cn (H. Wang).

maintain their integrity over several charge/discharge cycles and often suffered from rapid capacity fading due to their low conductivity, severe agglomeration problem, and serious volume expansion and contraction during charge and discharge processes [9,10].

To improve the stability of Fe_2O_3 electrodes and obtain better capacity retention and cycle life for Fe_2O_3, the introduction of carbonaceous materials has been generally accepted due to their high electronic conductivity, excellent buffering effect and mechanical strength. For the investigation of carbonaceous materials as modified elements, one effective way could be disperse Fe_2O_3 particles on a "carbon support" like graphite, carbon nanofibers (CNFs), carbon nanotubes (CNTs) or graphene nanosheets (GNs) to form Fe_2O_3/C type hybrid materials [11–14]. In these materials, however, Fe_2O_3 particles partially get in touch with the support by noncovalent force and some of them may peel off from their support during the synthesis or charge/discharge process. Another strategy is to design nano-scale carbon coating on the surface of Fe_2O_3 and thus to form Fe_2O_3@C core–shell type hybrid materials [15]. In these materials, however, the agglomeration of Fe_2O_3 cannot be solved satisfactorily.

Although the both modified methods have unavoidable drawbacks, each of these two approaches alone has been proved to be effective in improving the cycling performance of Fe_2O_3 or other metal oxides (M_xO_y) that can be used as anode materials [16–19]. Therefore, there comes to appear another challenge, to combine the carbon coating (defined as C_1) and the support (defined as C_2, C_2 = graphite, CNFs, CNTs or GNs) simultaneously in one material system to synthesize M_xO_y@C_1/C_2 type hybrid materials. When used as anode materials for LIBs, C_1 with good elasticity covered over the M_xO_y are expected to effectively accommodate the strain of volume change during lithium insertion/extraction and prevent the M_xO_y particles fall off from the electrode. C_2 in the hybrid are expected to become an efficient support or substrate material to disperse M_xO_y particles well, which further prevent the agglomeration of M_xO_y. It can be speculated that this type hybrids would overcome the drawbacks of M_xO_y-C_1 and M_xO_y-C_2, and thus obtain improved electrochemical performance as anode materials.

Considering the potential advantages of the M_xO_y@C_1/C_2 type materials, in this paper, a novel carbon-coated Fe_2O_3 submicroparticles loaded on GNs (Fe_2O_3@C/GNs) hybrid material was prepared by a two step route which including a hydrothermal and a subsequently glucose impregnation-pyrolysis process. The electrochemical performance of the hybrid material was evaluated, and as a result, the material exhibits much higher specific capacity and better cycling performance than that of bare Fe_2O_3 and Fe_2O_3/GNs materials as an anode material for LIBs.

2. Experimental section

2.1. Synthesis of the materials

GNs were prepared by a thermal exfoliation method involving graphite oxidation, followed by rapid thermal expansion under an Ar atmosphere. The detailed preparation procedure can be found in a previous paper [20].

For the preparation of Fe_2O_3/GNs: in a 50 ml beaker, 0.4 g $FeCl_3 \cdot 6H_2O$, 0.75 g polyvinylpyrrolidone (PVP) and 0.1 g CH_3COONH_4 were dissolved in a deionized water of 30 ml to get an orange solution. And then 30 mg GNs were added into the solution and sonicated for 2 h to yield a homogeneous suspension. The mixture was then transferred into a 50 ml Teflon-lined autoclave, heated at 140 °C in an electric oven for 24 h. After the autoclave cooled down, the resulting brownish black solid products were centrifuged, washed with deionized water and ethanol to remove the ions possibly remaining in the final products, and then dried at 80 °C under vacuum. For

comparison, Fe_2O_3 sample was synthesized following the same procedure except that no GNs were added.

For the preparation of Fe_2O_3@C/GNs: 0.6 g glucose was dissolved in deionized water (10 ml) until a clear solution was observed. 0.3 g Fe_2O_3/GNs was dispersed in another 10 ml deionized water by ultrasonication to form a suspension, and the former glucose solution and another 10 ml of ethanol were added to the suspension under gentle stir. After sonication in an ultrasonic bath for 2 h, the solid products was collected by filtration and then dried in a vacuum oven at 80 °C for 12 h, followed by heating in a tube furnace under Ar at 600 °C for 3 h.

2.2. Characterization

Powder X-ray diffraction (XRD) patterns were recorded by a Rigaku D-max C III X-ray diffractometer using Cu Kα radiation ($\lambda = 0.15418$ nm) at a scanning rate of 0.02° s^{-1} in the 2θ range from 20° to 60°. Thermogravimetric analysis (TG) was carried out on a NETZSCH STA 449C thermal analysis instrument, and the heating rate was 10 °C min^{-1}. Scanning electron microscopy (SEM) images were obtained on a JEOL JSM6700 F field-emission SEM. Transmission electron microscopy (TEM), and high-resolution TEM (HRTEM) images were obtained on a JEOL JEM-3010 instrument with an accelerating voltage of 200 kV.

2.3. Electrochemical measurements

The electrochemical measurements were performed at 25 °C using coin cells (CR2430) with pure lithium foil as the counter and reference electrode. The working electrode consists of a test material (e.g., Fe_2O_3, GNs, Fe_2O_3/GNs or Fe_2O_3@C/GNs), acetylene black and polytetrafluoroethylene (PTFE) in a weight ratio 80:10:10, and pasted on pure Cu mesh. The prepared working electrodes were dried in a vacuum oven at 100 °C over 12 h to remove the solvent. These electrodes had a solid loading of 5.0 mg cm^{-2}. Cells were constructed in a glove box in argon atmosphere under a dew point below −65°. The electrolyte was 1 M $LiPF_6$ dissolved in a mixture of dimethyl carbonate, diethyl carbonate and ethylene carbonate (1:1:1 by volume), and the separator was microporous polypropylene film. The cells were tested by galvanostatic charge/discharge tests and electrochemical impedance spectroscopy (EIS) measurements. The charge/discharge tests were carried out on LAND battery program-control test system (CT 2001A, Wuhan Jinnuo Electronic Co. Ltd. of China) at a constant current density of 200 mA g^{-1} in a cut-off voltage window of 0.005–3.0 V. EIS measurements were measured on an electrochemical workstation (660D, CHI company, China) with the frequency range from 0.01 Hz to 100 kHz.

3. Results and discussion

Fe_2O_3/GNs and Fe_2O_3@C/GNs were characterized by XRD (Fig. 1(a)). The typical peaks of α-Fe_2O_3 (JCPDS 33-0664) could be identified in the two samples. There is no obvious diffraction peak attributed to graphite in Fe_2O_3/GNs and Fe_2O_3@C/GNs, which indicates that the stacking of GNs in Fe_2O_3/GNs and Fe_2O_3@C/GNs and the carbon formed by glucose pyrolysis in Fe_2O_3@C/GNs are disordered. The TG analysis in Fig. 1(b) shows that the carbon content of Fe_2O_3@C/GNs is about 15%, which is a little higher than the GNs content in Fe_2O_3/GNs sample (about 10.5%). These results indicate that the amount of amorphous carbon converted by glucose is 4.5%. However, whether the formed amorphous carbon was successfully coated on Fe_2O_3, it needs SEM and TEM investigation to confirm.

The SEM micrographs of Fe_2O_3 particles, Fe_2O_3/GNs and Fe_2O_3@C/GNs are shown in Fig. 2. As shown in Fig. 2(a), Fe_2O_3
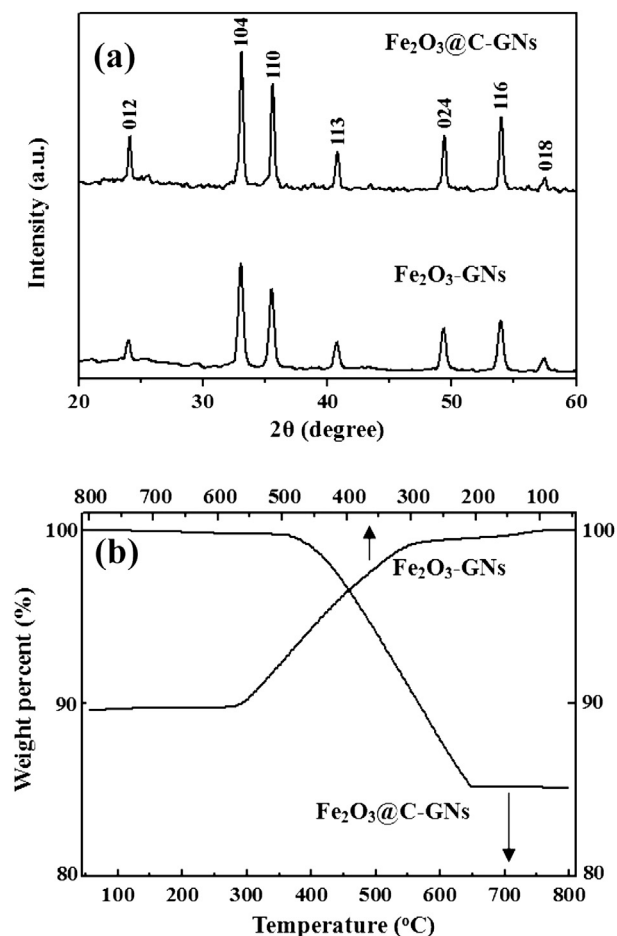
Fig. 1. (a) XRD patterns of Fe$_2$O$_3$/GNs and Fe$_2$O$_3$@C/GNs, (b) TG curves of Fe$_2$O$_3$-GNs and Fe$_2$O$_3$@C/GNs.

particles are of sphere like morphology in general, and the diameter of them is slightly different ranging from 400 to 420 nm. These Fe$_2$O$_3$ particles tend to aggregate with each other, which would lead to the poor cycling performance as an anode material for LIBs based on their conversion mechanism. After the introduction of GNs, it is clearly seen in Fig. 2(b) that the Fe$_2$O$_3$ submicro-particles with very few aggregations were dispersed on GN surface. For the Fe$_2$O$_3$@C/GNs sample in Fig. 2(c), it can be seen that there is no significant change in morphology when compared with Fe$_2$O$_3$/GNs, indicating the carbon formed by pyrolysis of glucose may be thin layer and is coated on the Fe$_2$O$_3$ particles.

The structural details of Fe$_2$O$_3$, Fe$_2$O$_3$/GNs and Fe$_2$O$_3$@C/GNs were analyzed by TEM and displayed in Figs. 3 and 4. Fig. 3(a) shows a Fe$_2$O$_3$ particle with spherical in shape and has a diameter of ∼400 nm, which is consistence with the result obtained from SEM measurement. Fig. 3(b) is a HRTEM image of the edge of the selected area Fe$_2$O$_3$ in Fig. 3(a). The clear lattice image indicates the high crystallization and single crystalline nature of the Fe$_2$O$_3$ spheres. The typical lattice fringe spacing was determined to be 0.375 nm, corresponding to the (012) plane of the crystal. Fig. 3(c) and (d) gives the low magnification TEM images of Fe$_2$O$_3$/GNs and Fe$_2$O$_3$@C/GNs hybrid materials, respectively. The morphology of the two materials is similar to each other: plenty of black particles randomly distributed on GNs. Note that there still exists a few particles observed which could not loaded on GNs successfully. Such a phenomenon often occurs over the M$_x$O$_y$-C$_2$ type hybrid materials and is mainly caused by the growth of M$_x$O$_y$ particles freely in the initial reaction system [21].

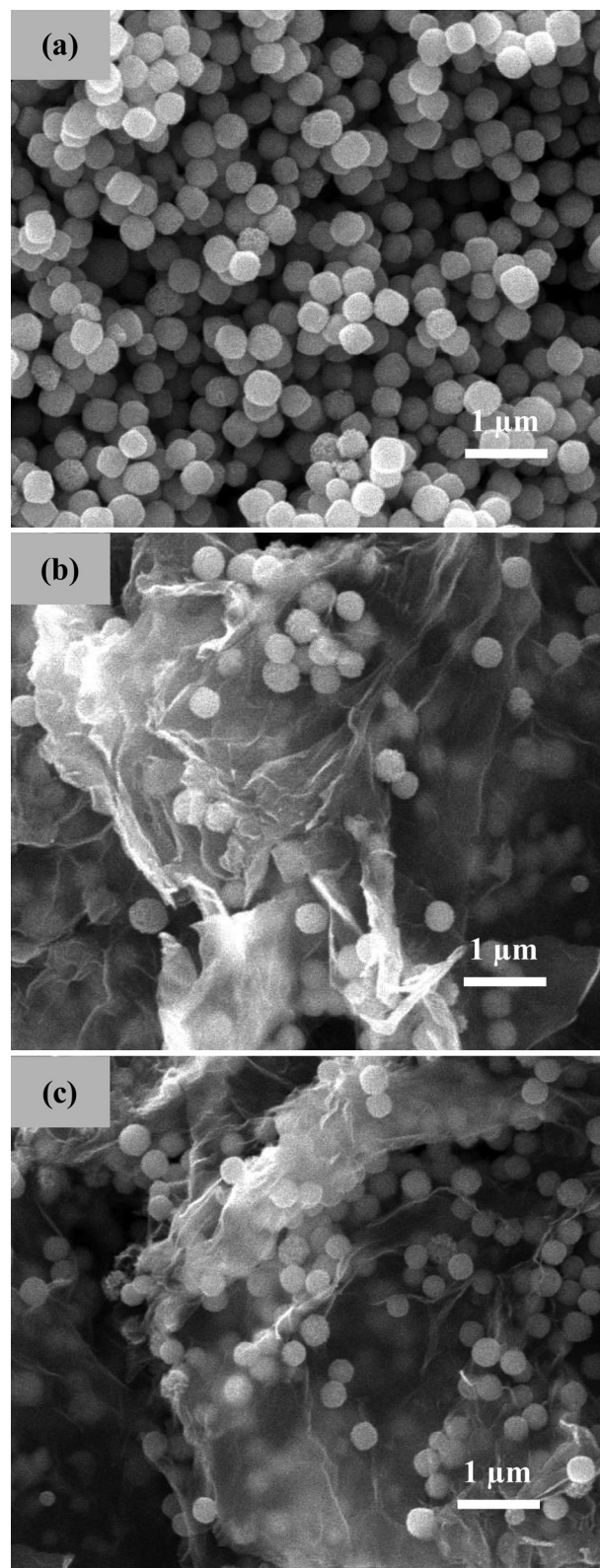Fig. 2. SEM images of (a) Fe$_2$O$_3$, (b) Fe$_2$O$_3$/GNs and (c) Fe$_2$O$_3$@C/GNs.

Fig. 4 gives a series of TEM images of the Fe$_2$O$_3$@C/GNs hybrid material. Fig. 4(a) shows a high magnification TEM image of an edge of the Fe$_2$O$_3$@C/GNs material. From it, the crumpled GNs could be seen clearly. Fig. 4(b) was recorded from the rectangle region in Fig. 4(a). The distinguishable lines in parallel in Fig. 4(b) correspond
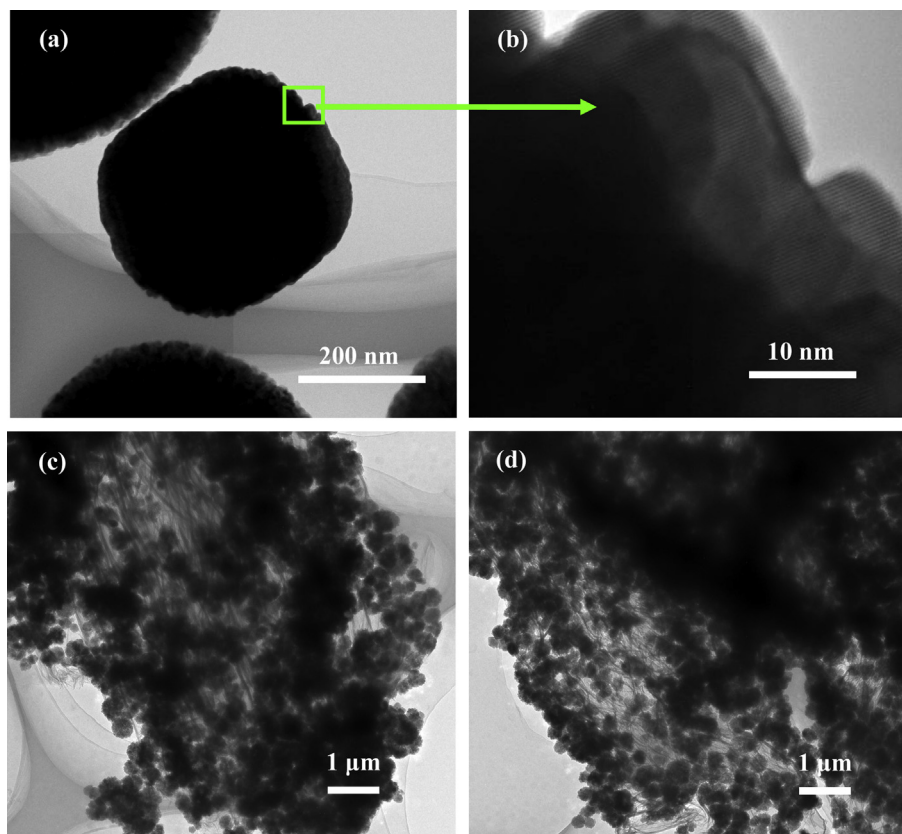
Fig. 3. (a) TEM and (b) HRTEM images of Fe_2O_3, TEM images of (c) Fe_2O_3/GNs and (d) Fe_2O_3@C/GNs hybrid materials.

to the fold of GNs, from which the number of layers can be estimated. Approximately 25–30 layers were identified by the fact that the graphene platelet thickness ranged from 8 to 10 nm. Fig. 4(c) is a TEM image of one single Fe_2O_3 derived from the Fe_2O_3@C/GNs material. The amorphous carbon is surrounding the edge of Fe_2O_3 and shows a shallow contrast in the image. HRTEM image of Fig. 4(d) clearly shows that the coated thin carbon layer with an average thickness of about 5 nm at the surface of Fe_2O_3, as marked with black arrow. Based on the above analysis, it can be confirmed that the final products is indeed carbon coated Fe_2O_3 loaded on the GN matrix.

The electrochemical performance of the Fe_2O_3@C/GNs material as an anode was investigated. And for comparison, the synthesized GNs, bare Fe_2O_3 and Fe_2O_3/GNs were also investigated under the same conditions. Fig. 5 shows the first electrochemical lithiation/delithiation of GNs, bare Fe_2O_3, Fe_2O_3/GNs and Fe_2O_3@C/GNs electrodes at the current density of 200 mA g^{-1}. The GN electrode (Fig. 5(a)) has an initial discharge capacity of 1669 mA h g^{-1} and charge capacity of 815 mA h g^{-1}, which corresponding to a low coulombic efficiency of 49%. Additionally, it shows a profile with a large charge/discharge voltage hysteresis without distinguishable plateaus. Such a phenomenon has also been demonstrated in other literature [22]. The features of charge and discharge curves of the other three electrodes (Fig. 5(b)) are similar to each other, and are in agreement with that of the reported Fe_2O_3 powder. The sloped region between 1.2 and 0.9 V is corresponding to the lithium insertion into the crystal structure of Fe_2O_3 and the conversion from Fe^{3+} to Fe^{2+}. The long plateau that appeared at ∼0.8 V is attributed to the conversion from Fe^{2+} to Fe^0 [9]. The charge curves show a sloping plateau at ∼1.8 V due to the reverse reaction. It also can be seen from Fig. 5(b) that the first cycle discharge capacities were 1288, 1475 and 1540 mA h g^{-1} for the electrodes of Fe_2O_3,

Fe_2O_3/GNs and Fe_2O_3@C/GNs, respectively, with the corresponding first cycle charge capacities of 706, 936 and 1100 mA h g^{-1}. Accordingly, the coulombic efficiencies were 55, 63 and 71% for Fe_2O_3, Fe_2O_3/GNs and Fe_2O_3@C/GNs, respectively. The result indicates that the initial coulombic efficiency of Fe_2O_3@C/GNs is significantly higher than GNs, bare Fe_2O_3 particles and Fe_2O_3/GNs material, showing a remarkable decrease of the irreversible capacity loss. The initial irreversible capacity of ∼440 mA h g^{-1} in the hybrid material could be attributed to the formation of solid electrolyte interface (SEI) layer and the decomposition of electrolyte, which are unavoidable for most anode materials [23].

Fig. 6 shows a comparison of the charge/discharge cyclic performance for GNs, bare Fe_2O_3, Fe_2O_3/GNs and Fe_2O_3@C/GNs materials at the current density of 200 mA g^{-1}. The GN electrode shows a high initial reversible capacity, which decreases gradually to 505 mA h g^{-1} after the cell has undergone 50 cycles. The corresponding capacity retention is 62%. For the Fe_2O_3 electrode, there was a rapid fading of capacity due to the particle aggregation and electrode pulverization. After 50 cycles, the capacity only remained 400 mA h g^{-1}, which is about 56% retention of the initial reversible capacity. The Fe_2O_3/GNs electrode demonstrates much better reversible capacity and cycle stability than that of the Fe_2O_3 and GN electrodes. After 50 cycles, the capacity still remained 740 mA h g^{-1}, the retention capacity rate was 79%. Regarding to the Fe_2O_3@C/GNs electrode, it shows a super high capacity of 900 mA h g^{-1} after 50 cycles and the capacity retention rate was a high 82%. The above results indicate that Fe_2O_3@C/GNs electrode could exhibit an improved reversible capacity and cycling stability compared to the Fe_2O_3, and Fe_2O_3/GNs electrodes.

EIS measurements were conducted to elucidate Li$^+$ and electron kinetics in Fe_2O_3, Fe_2O_3/GNs and Fe_2O_3@C/GNs electrodes. The Nyquist plots of the three electrodes before and after 50 cycles are
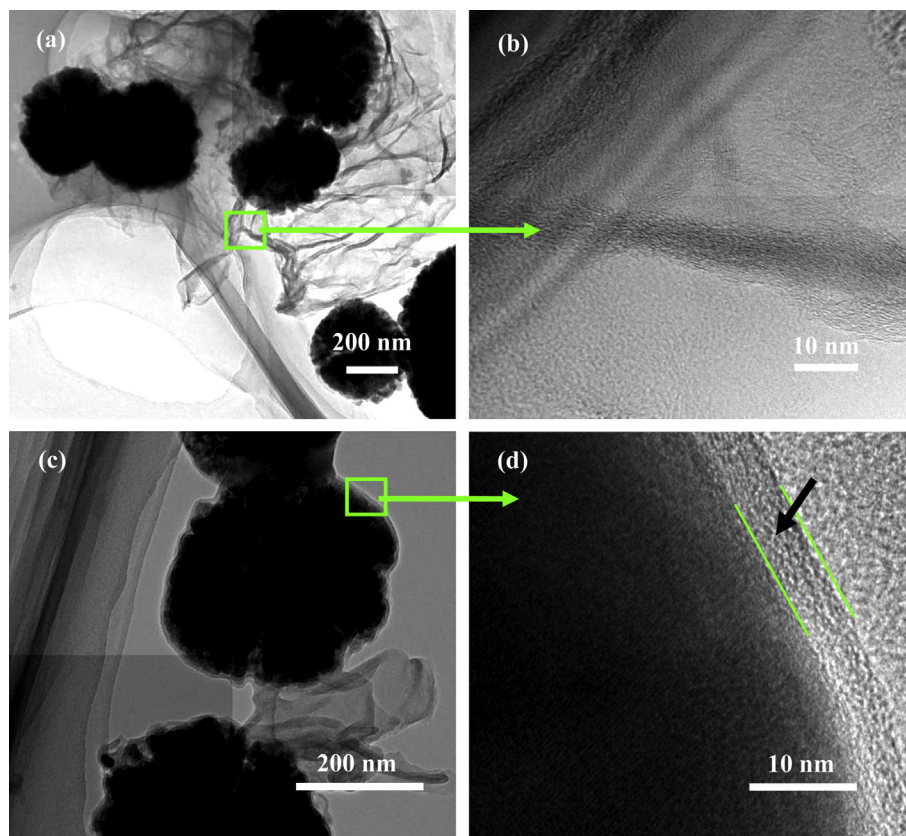
Fig. 4. (a) High magnification TEM image of an edge of the Fe$_2$O$_3$@C/GNs, (b) the selected area HRTEM image of the GNs, (c) TEM image of a single Fe$_2$O$_3$ derived from the Fe$_2$O$_3$@C/GNs, and (d) the selected area HRTEM image of the Fe$_2$O$_3$.

shown in Fig. 7. As can be observed from the figure, the shapes of Nyquist plots of the three electrodes are quite similar. Generally, the Nyquist plots consisted of a high-frequency semicircle, a medium-frequency semicircle and a low-frequency sloping straight line [24]. However, it is difficult to distinguish the two semicircles in the high- and medium-frequency region in Fig. 7, which may be due to a conjunction of the two semicircles. The semicircle at high-frequency region was related to the SEI film resistance. The semicircle at medium-frequency region was attributed to the lithium ion charge-transfer impedance on the electrode. And the straight line at low-frequency region represented the Warburg impedance, which was related to the diffusion-controlled process in the solid state electrodes. From Fig. 7, it can be clearly seen that the semicircle in the medium-frequency region for Fe$_2$O$_3$@C/GNs before cycling is much smaller than that of Fe$_2$O$_3$ (323 Ω), and a little smaller than that of Fe$_2$O$_3$/GNs (136 Ω), indicating the lowest charge-transfer resistance of Fe$_2$O$_3$@C/GNs (110 Ω). After 50 cycles, although the diameter of the semicircles at medium-frequency region was enlarged for all the electrodes (the related resistance for Fe$_2$O$_3$, Fe$_2$O$_3$/GNs and Fe$_2$O$_3$@C/GNs are742, 299 and 239 Ω, respectively), the lowest charge-transfer resistance can also be obtained on Fe$_2$O$_3$@C/GNs. In addition, it can be estimated from Fig. 7 that the increase value of the charge transfer resistance for Fe$_2$O$_3$, Fe$_2$O$_3$/GNs and Fe$_2$O$_3$@C/GNs electrodes after 50 cycles are 419, 163 and 129 Ω, respectively. Since the faradic reaction is determined by ion transfer and electron conduction, the reduction of the increase value for the resistance can be attributed to the improved electronic conductivity of the hybrid material induced by GNs and carbon coating layer, thus resulting in enhanced electrode reaction kinetics and better cycling performance of the cells [25].

In order to further understand the effects of the GNs and the coated carbon on the electrochemical performance of Fe$_2$O$_3$ particles, the surface morphology of the three electrodes, Fe$_2$O$_3$, Fe$_2$O$_3$/GNs and Fe$_2$O$_3$@C/GNs, before and after 50 cycles are measured by SEM, and displayed in Fig. 8. Fig. 8(a) reveals the surface of the Fe$_2$O$_3$ electrode before cycling. As shown in it, the surface of the Fe$_2$O$_3$ electrode was occupied by a large number of aggregated Fe$_2$O$_3$ spheres (white dots) together with a few formed Fe$_2$O$_3$ blocks. Fig. 8(b) and (c) shows the surface of the other two electrodes before cycling, different from the morphology shown in Fig. 8(a), it can be seen that the sphere-like particles are well dispersed on the electrodes without obvious aggregation. GNs in the two images could not observe significantly may be due to their sheet-like morphology and the fact that they have undergone a compression process with carbon black and PTFE. Combined the results obtained in Figs. 2 and 3, it can be concluded that the improvement of the two electrodes' surfaces (Fig. 8(b) and (c)) was mainly attributed to the introduction of GNs. Fig. 8(a'), (b') and (c') give the surface morphology of the three electrodes, Fe$_2$O$_3$, Fe$_2$O$_3$/GNs and Fe$_2$O$_3$@C/GNs, after 50 cycles. As can be seen in these SEM images, the three electrodes display entirely different surface morphologies. For the Fe$_2$O$_3$ electrode in Fig. 8(a'), the integrity of the electrode has been destroyed by the continuous charge and discharge process and the pulverization of the electrode occurred seriously. Plenty of Fe$_2$O$_3$ spheres have fallen off from the electrode because of the volume change during the repeated cycling process (see the inset figure in Fig. 8(a')) and have lost the electric contact with each other. The transfer of electrons and lithium ion in the interface of active materials and electrolyte was hindered and therefore a high charge-transfer resistance was
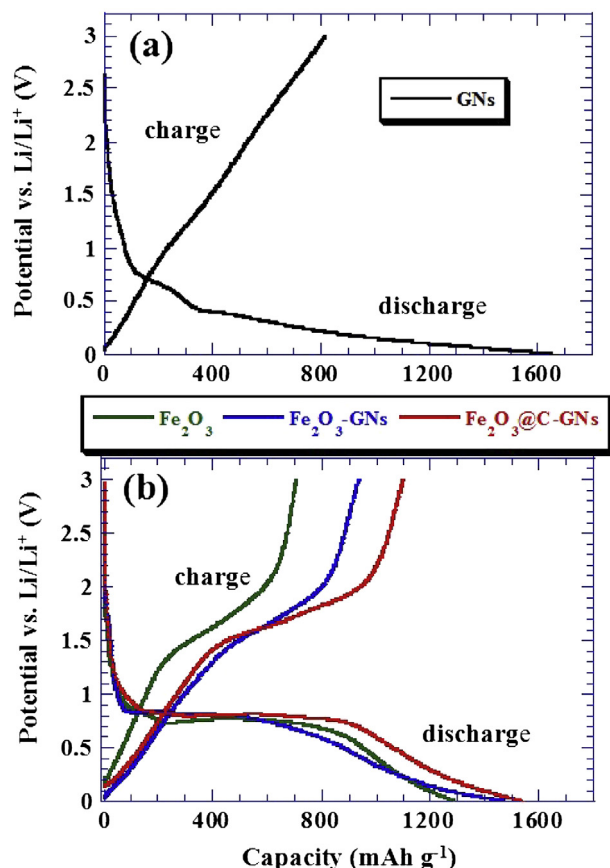
Fig. 5. Charge/discharge profiles of (a) GNs and (b) Fe_2O_3, Fe_2O_3/GNs and Fe_2O_3@C/GNs at the current density of 200 mA g^{-1}.

obtained, which finally lead to the poor lithium storage property of Fe_2O_3 electrode. Regarding to Fe_2O_3/GNs, although the GNs could well dispersed Fe_2O_3 particles and suppress the volume change of them to some extent, the structural integrity of Fe_2O_3/GNs in Fig. 8(b′) still destroyed obviously and part of the Fe_2O_3 particles peeled off from the electrode (see the inset figure in Fig. 8(b′)). Therefore, the Fe_2O_3/GNs exhibited a limited lithium storage capacity during the charge/discharge process. Considering the fact that Fe_2O_3 submicro-particles were randomly dispersed on GNs, it
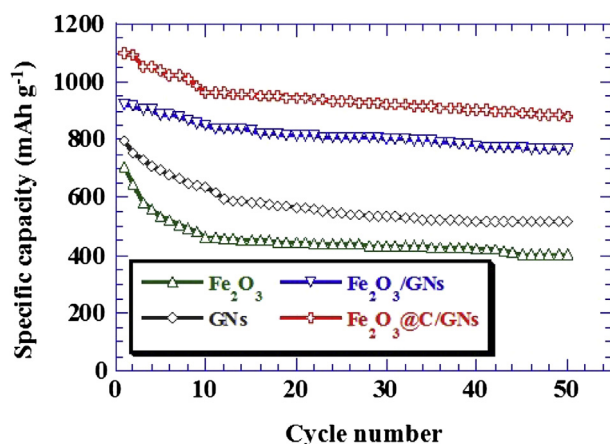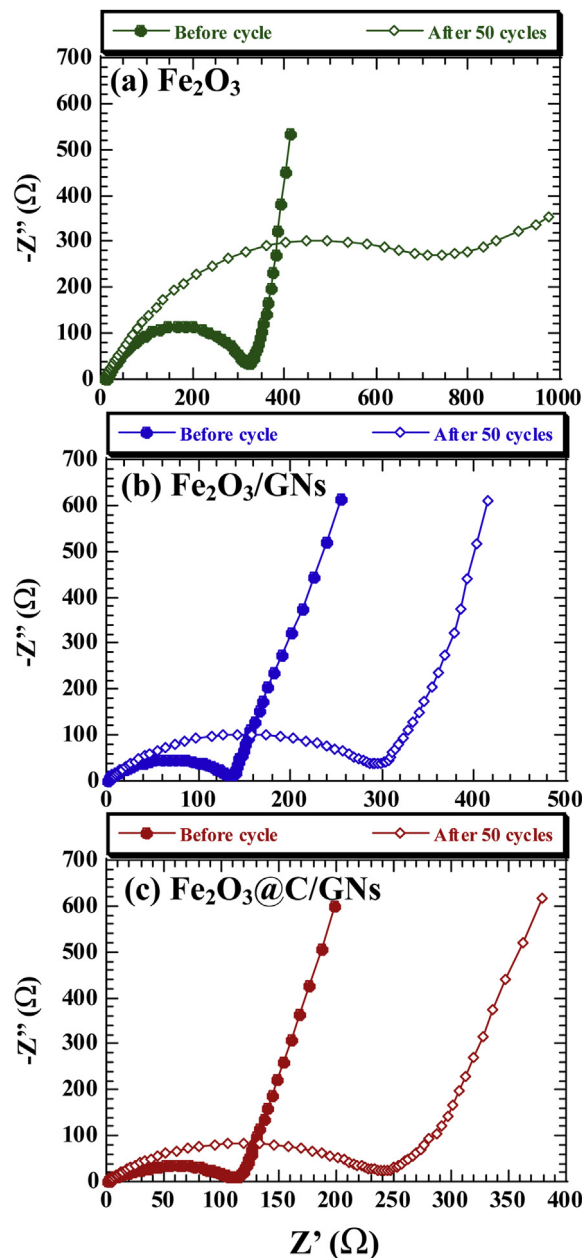

Fig. 7. The Nyquist plots of (a) Fe_2O_3, (b) Fe_2O_3/GNs and (c) Fe_2O_3@C/GNs electrodes before and after 50 cycles.

can be speculated that the following reasons may lead to the result: (1) the GNs can not buffer the volume change of Fe_2O_3 thoroughly; and (2) a few Fe_2O_3 particles which have not loaded on GNs have fallen off from the electrode during the charge/discharge process, just like what happened on the Fe_2O_3 electrode. Fig. 8(c′) shows the surface morphology of Fe_2O_3@C/GNs electrode after 50 cycles. It can be seen in the figure that the density of Fe_2O_3 per unit area in the electrode was just slightly decreased when compared with the result obtained before cycling and most of the Fe_2O_3 particles still adhere strongly to the electrode. Thus the integrity of the electrode was maintained in the main during the charge/discharge cycles. Such a situation could provide an excellent electrical contact between Fe_2O_3 spheres, and is good for the effective transport of electrons and lithium ion. As a result, the Fe_2O_3@C/GNs exhibited much better electrochemical performance than the Fe_2O_3 and Fe_2O_3/GNs materials.
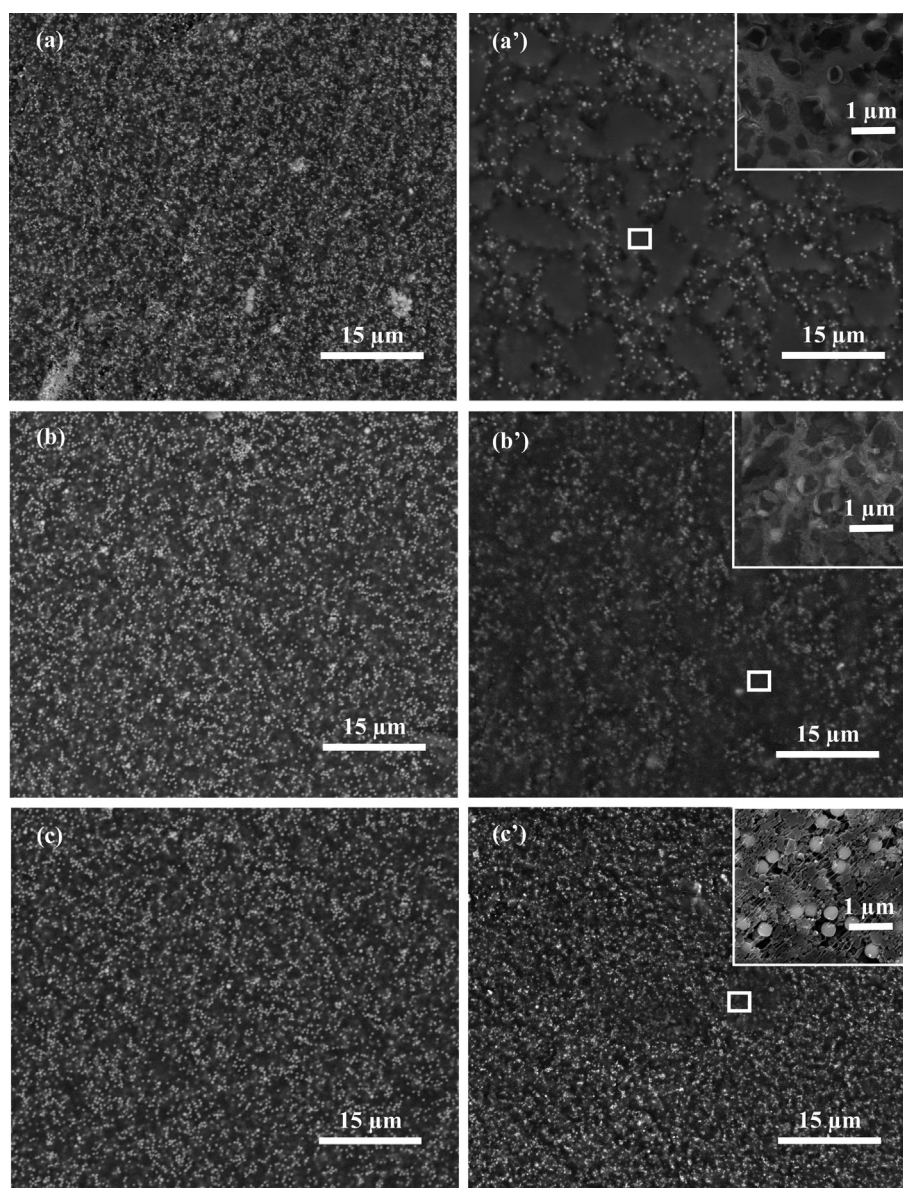

Fig. 6. Reversible lithium storage capacities vs. cycle number for Fe_2O_3, GNs, Fe_2O_3/GNs and Fe_2O_3@C/GNs electrodes.

Fig. 8. SEM images of Fe$_2$O$_3$ (a) before and (a′) after cycling, Fe$_2$O$_3$/GNs (b) before and (b′) after cycling, and Fe$_2$O$_3$@C/GNs (c) before and (c′) after cycling, respectively. The inset in Fig. 8(a′), (b′) and (c′) are the selected area high magnification SEM images.

Based on the above results, it is apparently the excellent electrochemical performance of Fe$_2$O$_3$@C/GNs can be attributed to the following factors. Firstly, it is well known that graphene possess capacity to store lithium ion. Thus GNs would contribute to the overall capacity of the hybrid material. The contribution of GNs to the overall capacity of the hybrid material is about 60 mA h g^{-1} (573 mA h g^{-1} × 10.5%, 573 is the average reversible capacity of GNs in 50 cycles) in view of their performance in Fig. 6. Secondly, based on the morphology characterization of the hybrid material, the agglomeration of Fe$_2$O$_3$ particles was minimized after the introduction of GNs, which provide sufficient contact area for the reaction of lithium intercalation to Fe$_2$O$_3$. Additionally, the incorporation of GNs and thin carbon layer around the particles can not only improve the electrical conductivity of the electrode, but also serve as a structural buffering layer to cushion the internal strain associated with lithium uptake while preventing the Fe$_2$O$_3$ particles from being electrically isolated upon, thus maintaining the integrity of the electrode. Benefited from the enhanced

structural stability and kinetics for lithium storage, the synergetic effect of GNs and coated carbon layer gives rise to the Fe$_2$O$_3$ possesses relatively higher capacity and capacity retention when compared with the Fe$_2$O$_3$ and Fe$_2$O$_3$/GNs material.

Although the hybrid material displayed high lithium storage property, it is still lower than some previously reported carbon modified Fe$_2$O$_3$ hybrid materials [13,14,23,26]. The reason may be related to the size of the Fe$_2$O$_3$ used. The synthesized Fe$_2$O$_3$ spheres have a diameter of ∼400 nm, much bigger than those reported high-performance nanomaterials (20–50 nm). It is well known that those M$_x$O$_y$ materials with nanosized dimensions often possess excellent electrochemical performance than microsized samples. Such results are mainly caused by their large surface areas and short lithium ion diffusion distances in nanomaterials [27]. Large surface areas of the nanosized samples permit a high contact area with the electrolyte and thus lead to high lithium ion flux across the interface of M$_x$O$_y$. Moreover, due to the short distances for lithium ion transport on nanosized materials, the reduced dimensions for

the samples can effectively increase the rate of lithium insertion/extraction. Based on the above discussion, it can be attributed to the submicro-sized dimension of the Fe_2O_3 for the lower lithium storage property of the hybrid material. Another problem is that the hybrid material exhibited limited cycling stability when compared to some other Fe_2O_3-carbon hybrid materials [23,26]. We believe the main reason is caused by the GNs introduced. GNs are an electroactive material for lithium storage and could contribute to the capacity of the overall electrode. However, similar to the non-graphitic carbons, when used as anode material, the lithium storage capacity of GNs often fades quickly [28]. Such a phenomenon can also be confirmed by the result in Fig. 6. After the introduction of GNs in the final products, it can be speculated that the cycling stability of the hybrid material would influence by GNs to some extent. Similar results can be found in other graphene-based anode materials [29–31]. According to the above discussions, further investigations are needed by tuning the size of Fe_2O_3 to nano-dimension or by improve the electrochemical performance of GNs.

4. Conclusions

A novel Fe_2O_3@C/GNs hybrid material was constructed by a two step route which including hydrothermal and the subsequently glucose impregnation-pyrolysis process. The hybrid exhibited an improved electrochemical performance compared with the Fe_2O_3 and Fe_2O_3/GNs materials when used as an anode material for LIBs. EIS measurements and the surface morphology contrast among the electrodes before and after cycling have confirmed that the combination of GNs and carbon coating over Fe_2O_3 is an effective way to improve the lithium storage property of Fe_2O_3. It can be easily extend this synthetic method to the preparation of other metal oxide-based anode materials.

Acknowledgements

References

[1] J.B. Goodenough, Y. Kim, Chem. Mater. 22 (2010) 587–603.
[2] G. Derrien, J. Hassoun, S. Panero, B. Scrosati, Adv. Mater. 19 (2007) 2336–2340.
[3] M. Yoshio, H. Wang, K. Fukuda, Angew. Chem. Int. Ed. 42 (2003) 4203–4206.
[4] P. Poizot, S. Laruelle, S. Grugeon, L. Dupont, J.M. Tarascon, Nature 407 (2000) 96–499.
[5] L. Ji, Z. Lin, M. Alcoutlabi, X. Zhang, Energy Environ. Sci. 4 (2011) 2682–2699.
[6] C.H. Jiang, E. Hosono, H.S. Zhou, Nano Today 1 (2006) 28–33.
[7] J. Chen, L. Xu, W. Li, X. Gou, Adv. Mater. 17 (2005) 582–586.
[8] H. Liu, G. Wang, J. Park, J. Wang, H. Liu, C. Zhang, Electrochim. Acta 54 (2009) 1733–1736.
[9] J. Zhong, C. Cao, Y. Liu, Y. Li, W.S. Khan, Chem. Commun. 46 (2010) 3869–3871.
[10] B. Sun, J. Horvat, H.S. Kim, W.S. Kim, J. Ahn, G. Wang, J. Phys. Chem. C 114 (2010) 18753–18761.
[11] B.T. Hang, S. Okada, J.L. Yamaki, J. Power Sources 178 (2008) 402–408.
[12] B.T. Hang, I. Watanabe, T. Doi, S. Okada, J.L. Yamaki, J. Power Sources 161 (2006) 1281–1287.
[13] X. Zhu, Y. Zhu, S. Murali, M.D. Stoller, R.S. Ruoff, ACS Nano 5 (2011) 3333–3338.
[14] G. Zhou, D.W. Wang, P.X. Hou, W. Li, N. Li, C. Liu, F. Li, H.M. Cheng, J. Mater. Chem. 22 (2012) 17942–17946.
[15] F. Cheng, K. Huang, S. Liu, J. Liu, R. Deng, Electrochim. Acta 56 (2011) 5593–5598.
[16] S.W. Lee, B.M. Gallant, H.R. Byon, P.T. Hammond, Y.S. Horn, Energy Environ. Sci. 4 (2011) 1972–1985.
[17] B. Luo, S. Liu, L. Zhi, Small 8 (2012) 630–646.
[18] Z.S. Wu, G. Zhou, L.C. Yin, W. Ren, F. Li, H.M. Cheng, Nano Energy 1 (2012) 107–131.
[19] H. Li, H. Zhou, Chem. Commun. 48 (2012) 1201–1217.
[20] D. Pan, S. Wang, B. Zhao, M. Wu, H. Zhang, Y. Wang, Z. Jiao, Chem. Mater. 21 (2009) 3136–3142.
[21] J. Yan, H. Song, S. Yang, J. Yan, X. Chen, Electrochim. Acta 53 (2008) 6351–6355.
[22] C. Wang, D. Li, C.O. Too, G.G. Wallace, Chem. Mater. 21 (2009) 2604–2606.
[23] A. Brandt, A. Balducci, J. Power Sources 230 (2013) 44–49.
[24] D. Zhang, Y.J. Mai, J.Y. Xiang, X.H. Xia, Y.Q. Qiao, J.P. Tu, J. Power Sources 217 (2012) 229–235.
[25] Q.Q. Xiong, Y. Lu, X.L. Wang, C.D. Gu, Y.Q. Qiao, J.P. Tu, J. Alloys Compd. 536 (2012) 219–225.
[26] Z. Wang, D. Luan, S. Madhavi, Y. Hu, X.W. Lou, Energy Environ. Sci. 5 (2012) 5252–5256.
[27] A.S. Arico, P. Bruce, B. Scrosati, J.M. Tarascon, W. Schalkwijk, Nat. Mater. 4 (2005) 366–377.
[28] P. Guo, H. Song, X. Chen, Electrochem. Commun. 11 (2009) 1320–1324.
[29] H. Kim, D.H. Seo, S.W. Kim, J. Kim, K. Kang, Carbon 49 (2011) 326–332.
[30] X. Zhu, Y. Zhu, S. Murali, M.D. Stoller, R.S. Ruoff, J. Power Sources 196 (2011) 6473–6477.
[31] Y. Jiang, T. Yuan, W. Sun, M. Yan, ACS Appl. Mater. Interfaces 4 (2012) 6216–6220.